

RESEARCH ARTICLE

[View Article Online](#)  
[View Journal](#) | [View Issue](#)



Cite this: *Inorg. Chem. Front.*, 2023, **10**, 5997

## Heteroanion-introduction-driven birefringence enhancement in oxychalcogenide $\text{Ba}_3\text{M}^{\text{II}}\text{Ge}_3\text{O}_2\text{S}_8$ ( $\text{M}^{\text{II}} = \text{Mn, Cd}$ )†

Sheng-Hua Zhou,<sup>‡a,b,c</sup> Mao-Yin Ran,<sup>‡a,b,c</sup> Wen-Bo Wei,<sup>a,b,c</sup> A-Yang Wang,<sup>a,b,d</sup> Xin-Tao Wu,<sup>‡a,b</sup> Hua Lin<sup>‡a,b</sup> and Qi-Long Zhu<sup>‡a,b</sup>

Birefringent crystals play a crucial role in regulating the polarization of light and are widely used in optoelectronic fields. However, the effective design of novel infrared (IR) birefringent crystals with large birefringence ( $\Delta n$ ) still face significant challenges. In this study, we present the rational design and successful synthesis of two novel quinary oxychalcogenides with the formula  $\text{Ba}_3\text{M}^{\text{II}}\text{Ge}_3\text{O}_2\text{S}_8$  ( $\text{M}^{\text{II}} = \text{Mn, Cd}$ ), employing a heteroanion-introduction strategy via high-temperature solid-state reactions.  $\text{Ba}_3\text{M}^{\text{II}}\text{Ge}_3\text{O}_2\text{S}_8$  ( $\text{M}^{\text{II}} = \text{Mn, Cd}$ ) crystallized in the monoclinic space group  $P2_1/n$  (no. 14) and the structures comprised one-dimensional (1D)  $[\text{M}^{\text{II}}\text{Ge}_3\text{S}_8\text{O}_2]^{6-}$  chains arranged in an antiparallel manner and separated by  $\text{Ba}^{2+}$  cations. The coexistence of multiple heteroanionic ligands ( $[\text{M}^{\text{II}}\text{OS}_5]$  octahedra,  $[\text{GeOS}_3]$ , and  $[\text{GeO}_2\text{S}_2]$  tetrahedra) in one material was surprisingly discovered for the first time in the realm of oxychalcogenides. It was revealed that the heteroanion-introduction strategy not only leads to a reduction in the structural dimensionality but also enhances the optical anisotropy significantly. Notably,  $\text{Ba}_3\text{M}^{\text{II}}\text{Ge}_3\text{O}_2\text{S}_8$  ( $\text{M}^{\text{II}} = \text{Mn, Cd}$ ) demonstrated large  $\Delta n$  values of 0.11 and 0.14, which represent a remarkable improvement compared to the three-dimensional (3D) parent  $\text{AE}_3\text{M}^{\text{II}}\text{M}^{\text{IV}}_2\text{Q}_8$  system ( $\Delta n = 0$ ). Furthermore, theoretical calculations suggest that the significant  $\Delta n$  of  $\text{Ba}_3\text{M}^{\text{II}}\text{Ge}_3\text{O}_2\text{S}_8$  ( $\text{M}^{\text{II}} = \text{Mn, Cd}$ ) resulted primarily from the combination of polarizabilities from the various heteroanionic groups. Overall, these results highlight the potential of the heteroanion-introduction strategy for designing novel IR birefringent materials for optoelectronic applications.

Received 26th July 2023,  
Accepted 23rd August 2023

DOI: 10.1039/d3qi01456h  
[rsc.li/frontiers-inorganic](http://rsc.li/frontiers-inorganic)

## 1. Introduction

Birefringent crystals play a crucial role in high-performance optics, especially in polarization apparatus, phase-matching elements, and laser processing.<sup>1</sup> Currently, the majority of the commercially available birefringent crystals are inorganic oxides, such as  $\text{YVO}_4$ ,<sup>2</sup>  $\text{CaCO}_3$ ,<sup>3</sup> and  $\alpha\text{-BaB}_2\text{O}_4$ .<sup>4</sup> However, these materials have their limitations. For instance, they suffer from detrimental metal–oxygen (M–O) bond absorptions, which

restrict their usage in the infrared (IR) region. Conversely, the current commercially available birefringent crystals are suitable for the ultraviolet and visible region, and few birefringent crystals have been explored for the IR region. In addition, the excellent birefringence ( $\Delta n$ ) of crystals enables the downsizing of crystal optical devices.<sup>5</sup> Consequently, there is an increasing demand for high-performance IR birefringent crystals in both the scientific research and technological development fields.

The analysis of the structure–property relationships of birefringent crystals revealed a positive correlation between the  $\Delta n$  and anisotropy.<sup>6</sup> In other words, a larger anisotropy corresponds to a greater  $\Delta n$ . Effective structural design strategies can be employed to modulate the  $\Delta n$ , such as introducing  $\pi$ -conjugated units,<sup>7</sup> stereochemically active lone pairs (SCALPs),<sup>8</sup> and functional building units (FBUs) with large polarizability anisotropy.<sup>9</sup> Recently, the heteroanion-introduction strategy has been proved to be an effective and direct approach for boosting the  $\Delta n$ , such as  $\text{Rb}_2\text{VO}(\text{O}_2)_2\text{F}$  ( $\Delta n = 0.189$  @ 546 nm),<sup>10</sup>  $\text{Sn}_2\text{BO}_3\text{I}$  ( $\Delta n = 0.393$  @ 546 nm),  $\text{Sn}_2\text{PO}_4\text{I}$  ( $\Delta n = 0.664$  @ 546 nm),<sup>11</sup>  $\text{RbTeMo}_2\text{O}_8\text{F}$  ( $\Delta n = 0.263$  @ 546 nm),<sup>12</sup> and  $\text{K}_2\text{Sb}(\text{P}_2\text{O}_7)\text{F}$  ( $\Delta n = 0.157$  @ 546 nm).<sup>13</sup>

<sup>a</sup>State Key Laboratory of Structural Chemistry, Fujian Institute of Research on the Structure of Matter, Chinese Academy of Sciences, Fuzhou 350002, China.

E-mail: [linhua@fjirsm.ac.cn](mailto:linhua@fjirsm.ac.cn), [qlzhu@fjirsm.ac.cn](mailto:qlzhu@fjirsm.ac.cn)

<sup>b</sup>Fujian Science & Technology Innovation Laboratory for Optoelectronic Information of China, Fuzhou, Fujian 350108, China

<sup>c</sup>University of Chinese Academy of Sciences, Beijing 100049, China

<sup>d</sup>College of Chemistry, Fuzhou University, Fuzhou 350002, China

† Electronic supplementary information (ESI) available: Additional experimental and theory results, together with additional tables and figures. CCDC 2234468 and 2234469. For ESI and crystallographic data in CIF or other electronic format see DOI: <https://doi.org/10.1039/d3qi01456h>

‡ These authors contributed equally to this work.

Oxychalcogenides with rich structures, varying from isolated zero-dimensional (0D) to dense three-dimensional (3D) frameworks, are an exciting class of heteroanionic system that have attracted significant attention in recent years owing to their high  $\Delta n$ , which can be obtained by partial anion substitution from the parent structure.<sup>14</sup> Some examples include  $\text{Ba}_3\text{Ge}_2\text{O}_4\text{Te}_3$  (0.14 @ 2090 nm, maternal structure:  $\text{Ba}_2\text{ZnGe}_2\text{O}_7$ ),<sup>15</sup>  $\text{SrGeOSe}_2$  (0.16 @ 2050 nm, maternal structure:  $\text{SrGeO}_3$ ),<sup>16</sup>  $\text{Sr}_2\text{CdGe}_2\text{OS}_6$  (0.193 @ 2050 nm, maternal structure:  $\text{Sr}_2\text{CdGe}_2\text{O}_7$ ),<sup>17</sup>  $\text{Nd}_3[\text{Ga}_3\text{O}_3\text{S}_3][\text{Ge}_2\text{O}_7]$  (0.091 @ 2050 nm, maternal structure:  $\text{Cs}_3[\text{Sb}_3\text{O}_6][\text{Ge}_2\text{O}_7]$ ),<sup>18</sup> and  $\text{Sr}_2\text{ZnSn}_2\text{OS}_6$  (0.12 @ 2050 nm, maternal structure:  $\text{Sr}_2\text{ZnSi}_2\text{O}_7$ ).<sup>19</sup> The parent structures mentioned above are all oxides. However, no examples have been reported using chalcogenides as parent structures to generate new oxychalcogenides by introducing oxygen atoms.

The quaternary  $\text{AE}_3\text{M}^{\text{II}}\text{M}^{\text{IV}}_2\text{Q}_8$  ( $\text{AE} = \text{Sr, Ba}$ ;  $\text{M}^{\text{II}} = \text{divalent transition metals}$ ;  $\text{M}^{\text{IV}} = \text{Ge, Sn}$ ;  $\text{Q} = \text{chalcogen}$ ) family is a complex system that distinguishes itself as an intriguing nonlinear optical (NLO) system owing to its structural flexibility at every crystallographic site.<sup>20</sup> However, its crystallization in the cubic space group results in the  $\Delta n$  values of 0, rendering it incapable of achieving phase-matching in NLO applications. Inspired by the previous strategy of introducing heteroanions, we successfully obtained two new oxychalcogenides, *i.e.*  $\text{Ba}_3\text{M}^{\text{II}}\text{Ge}_3\text{O}_2\text{S}_8$  ( $\text{M}^{\text{II}} = \text{Mn, Cd}$ ). In this study, the syntheses, structures, optical properties, and birefringent characteristics of the title compounds are described. Furthermore, theoretical calculations were conducted to achieve a better understanding of the structure–activity relationships.

## 2. Results and discussion

In the structure of  $\text{AE}_3\text{M}^{\text{II}}\text{M}^{\text{IV}}_2\text{Q}_8$ , the  $[\text{M}^{\text{IV}}\text{Q}_4]$  tetrahedron links 3  $[\text{M}^{\text{II}}\text{Q}_4]$  tetrahedra while  $[\text{M}^{\text{II}}\text{Q}_4]$  links 4  $[\text{M}^{\text{IV}}\text{Q}_4]$  tetrahedra to build up a 3D framework. Inside this framework, charge-balanced  $\text{AE}^{2+}$  cations are located in the cavity (Fig. 1a and c). Unfortunately, the dense 3D structure, which crystallizes in the cubic system (space group  $I\bar{4}3d$  (no. 220)), has an inappropriate anisotropy, resulting in a  $\Delta n$  value of 0 for  $\text{AE}_3\text{M}^{\text{II}}\text{M}^{\text{IV}}_2\text{Q}_8$ , and thereby rendering phase-matching impossible. It is widely recognized that the anisotropic polarization of a structure significantly impacts its  $\Delta n$ . Hence, the search for low-dimensional structures exhibiting significant anisotropy is considered one of the most effective means to obtain materials with a large  $\Delta n$ .<sup>21</sup>

The oxychalcogenides  $\text{Ba}_3\text{M}^{\text{II}}\text{Ge}_3\text{O}_2\text{S}_8$  ( $\text{M}^{\text{II}} = \text{Mn, Cd}$ ) represent a novel type of quinary compound discovered in  $\text{AE}/\text{M}^{\text{II}}/\text{M}^{\text{IV}}/\text{Q}/\text{O}$  systems. These compounds crystallize in the centrosymmetric monoclinic space group  $P2_1/n$  (no. 14); their detailed crystallographic information is shown in Table 1. The asymmetric unit consists of three independent Ba sites, one independent  $\text{M}^{\text{II}}$  site, three independent Ge sites, two independent O sites, and eight independent S sites. All the independent atom sites are located in the Wyckoff position 4e. The

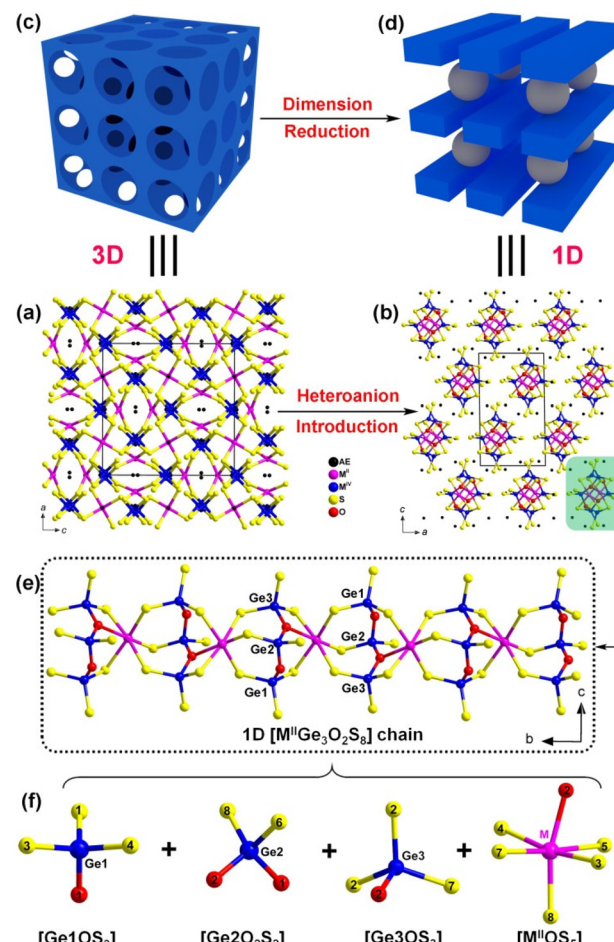


Fig. 1 Structural evolution from 3D  $\text{AE}_3\text{M}^{\text{II}}\text{M}^{\text{IV}}_2\text{Q}_8$  to 1D  $\text{Ba}_3\text{M}^{\text{II}}\text{Ge}_3\text{O}_2\text{S}_8$ : (a and b) ball-and-stick models viewed from the  $ac$ -plane; (c and d) schematic diagram of equivalent models; (e) projection of the 1D  $[\text{MGe}_3\text{O}_2\text{S}_8]^{6-}$  chain along the  $bc$ -plane; (f) coordination environment of  $[\text{GeOS}_3]$ ,  $[\text{GeO}_2\text{S}_2]$ , and  $[\text{M}^{\text{II}}\text{OS}_5]$  ( $\text{M}^{\text{II}} = \text{Mn, Cd}$ ) FBUs with the atom numbers marked.

basic structure of  $\text{Ba}_3\text{M}^{\text{II}}\text{Ge}_3\text{O}_2\text{S}_8$  can be seen as composed of 1D  $[\text{M}^{\text{II}}\text{Ge}_3\text{O}_2\text{S}_8]^{6-}$  infinite chains, while  $\text{AE}^{2+}$  cations fill the space to balance the charge (refer to Fig. 1b and d). The coordination environments of Ge and M<sup>II</sup> atoms are shown in Fig. 1f, and the key bond distances and angles are given in Table S1.<sup>†</sup> Ge1 and Ge3 atoms are linked to 1 O atom and 3 S atoms, forming heteroanionic  $[\text{GeOS}_3]$  FBUs with Ge–S bond lengths in the regular range of 2.174–2.205 Å and Ge–O bond distances of 1.806–1.838 Å. The Ge2 atom, on the other hand, is linked to 2 O atoms and 2 S atoms, forming heteroanionic  $[\text{GeO}_2\text{S}_2]$  FBUs with Ge–S bond lengths in the range of 2.137–2.178 Å and Ge–O bond lengths in the range of 1.779–1.787 Å. The M<sup>II</sup> atom is coordinated with 1 O and 5 S atoms to form a highly distorted  $[\text{M}^{\text{II}}\text{OS}_5]$  octahedron, with M<sup>II</sup>–S and M<sup>II</sup>–O bond lengths falling within the normal ranges.<sup>22</sup> Two  $[\text{GeOS}_3]$  FBUs and one  $[\text{GeO}_2\text{S}_2]$  FBU form a  $[\text{Ge}_3\text{O}_2\text{S}_8]$  cluster through bridging O atoms. These clusters are then interconnected with octahedral  $[\text{M}^{\text{II}}\text{OS}_5]$  FBUs, resulting

**Table 1** Crystal data and structural refinement details for  $\text{Ba}_3\text{M}^{\text{II}}\text{Ge}_3\text{O}_2\text{S}_8$  ( $\text{M}^{\text{II}} = \text{Mn, Cd}$ )

Empirical formula	$\text{Ba}_3\text{CdGe}_3\text{O}_2\text{S}_8$	$\text{Ba}_3\text{MnGe}_3\text{O}_2\text{S}_8$
CCDC	2234469	2234468
Formula weight	1030.67	973.21
Temperature (K)	293(2)	293(2)
Crystal system	Monoclinic	Monoclinic
Crystal color	Light yellow	Light yellow
Size (mm <sup>3</sup> )	0.08 × 0.10 × 0.10	0.07 × 0.10 × 0.11
Space group	$P2_1/n$ (no. 14)	$P2_1/n$ (no. 14)
$a$ (Å)	8.8294(10)	8.8298(7)
$b$ (Å)	11.9334(13)	11.8254(11)
$c$ (Å)	15.2993(17)	15.2442(11)
$\beta$ (°)	90.839(2)	90.548(7)
$V$ (Å <sup>3</sup> )	1611.8(3)	1591.7(2)
$Z$	4	4
$D_c$ (g cm <sup>-3</sup> )	4.247	4.061
$\mu$ (mm <sup>-1</sup> )	15.037	14.684
GOOF on $R^2$	1.139	1.119
$R_1, wR_2$ ( $I > 2\sigma(I)$ ) <sup>a</sup>	0.0265, 0.0720	0.0456, 0.1248
$R_1, wR_2$ (all data)	0.0290, 0.0725	0.0483, 0.1233
Largest diff. peak and hole (e Å <sup>-3</sup> )	1.512, -1.727	2.520, -1.257

$$^a R_1 = \sum ||F_o| - |F_c|| / \sum |F_o|, wR_2 = [\sum w(F_o^2 - F_c^2)^2 / \sum w(F_o^2)^2]^{1/2}.$$

in the formation of 1D  $[\text{M}^{\text{II}}\text{Ge}_3\text{O}_2\text{S}_8]^{6-}$  infinite chains through face-sharing (Fig. 1e). The Ba atoms also have different coordination behaviors. For instance, Ba1 and Ba3 atoms are surrounded by 8 S atoms, forming a  $[\text{BaS}_8]$  bicapped trigonal prism. On the other hand, the Ba2 atom is surrounded by 1 O atom and 7 S atoms, resulting in a more twisted  $[\text{BaOS}_7]$  bicapped trigonal prism (Fig. S1 and S2†).

The detailed structural evolution from 3D  $\text{AE}_3\text{M}^{\text{II}}\text{M}_2^{\text{IV}}\text{Q}_8$  to 1D  $\text{Ba}_3\text{M}^{\text{II}}\text{Ge}_3\text{O}_2\text{S}_8$  is depicted in Fig. 1. The introduction of O atoms, which have a different electronegativity ( $\chi_{\text{O}} = 3.44$  vs.  $\chi_{\text{S}} = 2.58$ ), can be viewed as acting like structural scissors to break the dense high-dimensional framework structure, resulting in the formation of a loosely connected low-dimensional chain structure. Consequently, a significantly anisotropic structure was obtained. This could be further confirmed by the experimental results and theoretical research on birefringence discussed in the following section.

Furthermore, through comparing and analyzing the reported oxychalcogenides, we discovered that  $\text{Ba}_3\text{M}^{\text{II}}\text{Ge}_3\text{O}_2\text{S}_8$  ( $\text{M}^{\text{II}} = \text{Mn, Cd}$ ) demonstrated structural novelty in three distinct aspects. First, the heteroanionic  $[\text{GeO}_x\text{Q}_{4-x}]$  FBUs can only exist in a singular form in oxychalcogenides,<sup>23–28</sup> such as  $[\text{GeOTE}_3]$ ,  $[\text{GeO}_2\text{S}_2]$ , and  $[\text{GeO}_3\text{Se}]$ , identified in  $\text{AE}_3\text{Ge}_2\text{O}_4\text{Te}_3$ ,<sup>15,23</sup>  $\text{AEGeOS}_2$ ,<sup>25</sup> and  $\text{Sr}_3\text{Ge}_2\text{O}_4\text{Se}_3$ ,<sup>27</sup> respectively. However, the title compounds simultaneously contained two  $[\text{GeO}_x\text{S}_{4-x}]$  FBUs, namely,  $[\text{GeOS}_3]$  and  $[\text{GeO}_2\text{S}_2]$ . Second, it has been reported that there are relatively few oxychalcogenides with transition-metal-based  $[\text{TMO}_x\text{Q}_y]$  FBUs,<sup>29</sup> but some examples include  $[\text{ZnO}_2\text{S}_2]$  in  $\text{BaZnOS}$ ,<sup>30</sup>  $[\text{ZnOS}_3]$  in  $\text{SrZn}_2\text{S}_2\text{O}$ ,<sup>31</sup>  $[\text{CoO}_2\text{S}_2]$  in  $\text{BaCoOS}$ ,<sup>32</sup> and  $[\text{CoOS}_3]$  in  $\text{CaCoOS}$ .<sup>33</sup> Notably, in contrast to the previously reported four-coordinated  $[\text{TMO}_x\text{Q}_y]$ , two new heteroanionic FBUs,  $[\text{MnOS}_5]$  and  $[\text{CdOS}_5]$ , were successfully observed in  $\text{Ba}_3\text{M}^{\text{II}}\text{Ge}_3\text{O}_2\text{S}_8$  ( $\text{M}^{\text{II}}$

= Mn, Cd) for the first time, which enhances the diversity of oxychalcogenides. Third, compounds with two or more heteroanionic FBUs are currently very rare, with the few examples limited to  $\text{Ba}_6\text{V}_4\text{O}_5\text{S}_{11}$  ( $[\text{VOS}_3] + [\text{VO}_2\text{S}_2]$ )<sup>34</sup> and  $(\text{Ba}_{19}\text{Cl}_4)(\text{Ga}_6\text{Si}_{12}\text{O}_{42}\text{S}_8)$  ( $[\text{GaOS}_3] + [\text{GaO}_2\text{S}_2]$ ).<sup>35</sup> The coexistence of multiple heteroanionic FBUs (octahedral  $[\text{M}^{\text{II}}\text{OS}_5]$ , tetrahedral  $[\text{GeOS}_3]$  and  $[\text{GeO}_2\text{S}_2]$ ) in the title compounds was surprisingly discovered for the first time in the realm of oxychalcogenides.

The compounds  $\text{Ba}_3\text{M}^{\text{II}}\text{Ge}_3\text{O}_2\text{S}_8$  ( $\text{M}^{\text{II}} = \text{Mn, Cd}$ ) were synthesized using a traditional high-temperature solid-state method. Single crystals with a millimeter-size were carefully selected for characterization and measurement (Fig. 2). The elemental analysis of  $\text{Ba}_3\text{M}^{\text{II}}\text{Ge}_3\text{O}_2\text{S}_8$  ( $\text{M}^{\text{II}} = \text{Mn, Cd}$ ) confirmed the symmetrical distribution through EDX mapping, and the  $\text{Ba} : \text{M}^{\text{II}} : \text{Ge} : \text{O} : \text{S}$  ratio was found to be highly consistent with the results obtained from single-crystal XRD (Fig. S3 and S4†). The purity phase of  $\text{Ba}_3\text{M}^{\text{II}}\text{Ge}_3\text{O}_2\text{S}_8$  ( $\text{M}^{\text{II}} = \text{Mn, Cd}$ ) was examined by powder XRD measurements (see Fig. 2a and b). The experimental results matched well with the simulated patterns derived from the single-crystal XRD measurements. The UV-Vis-NIR diffuse reflectance spectrum revealed optical energy gap ( $E_g$ ) values of 3.82 and 3.39 eV for  $\text{Ba}_3\text{CdGe}_3\text{O}_2\text{S}_8$  and  $\text{Ba}_3\text{MnGe}_3\text{O}_2\text{S}_8$  (Fig. 2c and d), respectively, using the Kubelka-Munk function.<sup>36</sup> These values are higher compared to other reported TM-based oxychalcogenides, such as  $\text{Sr}_6\text{Cd}_2\text{Sb}_6\text{O}_7\text{S}_{10}$  (1.89 eV),<sup>37</sup>  $\text{Sm}_3\text{NbS}_3\text{O}_4$  (2.68 eV),<sup>38</sup> and  $[\text{Sr}_3\text{VO}_4][\text{InSe}_3]$  (2.62 eV).<sup>39</sup> Additionally,  $\text{Ba}_3\text{M}^{\text{II}}\text{Ge}_3\text{S}_8\text{O}_2$  ( $\text{M}^{\text{II}} = \text{Mn, Cd}$ ) exhibited high thermal stability up to 1100 K under a  $\text{N}_2$  atmosphere based on the thermal analysis (Fig. S5†). There were no melting or phase transition behaviors observed in the corresponding DSC curves, which was consistent with the powder XRD results (Fig. S6†). Furthermore,  $\text{Ba}_3\text{CdGe}_3\text{O}_2\text{S}_8$  ( $\text{M}^{\text{II}} = \text{Mn, Cd}$ ) demonstrated a broad IR transmission cut-off

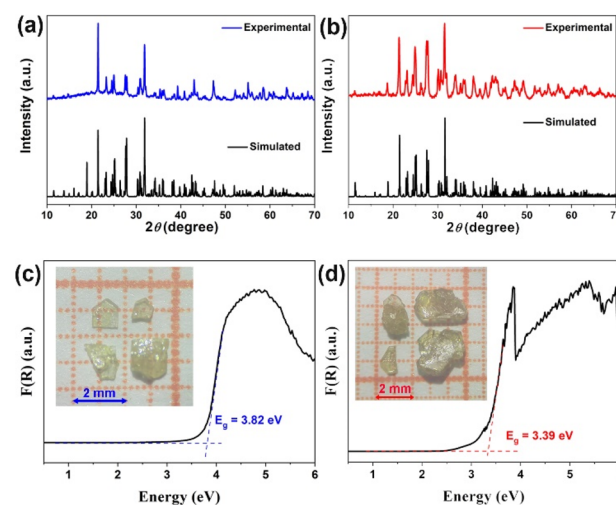


**Fig. 2** Characterization of  $\text{Ba}_3\text{M}^{\text{II}}\text{Ge}_3\text{O}_2\text{S}_8$  ( $\text{M}^{\text{II}} = \text{Mn, Cd}$ ): experimental and simulated powder XRD patterns for the as-synthesized (a)  $\text{Ba}_3\text{CdGe}_3\text{S}_8\text{O}_2$  and (b)  $\text{Ba}_3\text{MnGe}_3\text{S}_8\text{O}_2$ ; optical  $E_g$  for (c)  $\text{Ba}_3\text{CdGe}_3\text{S}_8\text{O}_2$  and (d)  $\text{Ba}_3\text{MnGe}_3\text{S}_8\text{O}_2$  (inset: optical images of the target single crystals).

region from 2.5 to 13.3  $\mu\text{m}$  (Fig. S7†), indicating their potential as IR birefringent candidates.

Inspired by oxychalcogenides that exhibit an appropriate  $\Delta n$  value,<sup>40</sup> the  $\Delta n$  of  $\text{Ba}_3\text{CdGe}_3\text{O}_2\text{S}_8$  ( $\text{M}^{\text{II}} = \text{Mn, Cd}$ ) was also measured using a ZEISS Axio A1 cross-polarizing microscope. The retardations ( $R$  values) and crystal thicknesses ( $T$  values) were tested as 1.073  $\mu\text{m}$  and 9.8  $\mu\text{m}$  for  $\text{Ba}_3\text{MnGe}_3\text{O}_2\text{S}_8$ , and 0.85  $\mu\text{m}$  and 5.9  $\mu\text{m}$  for  $\text{Ba}_3\text{CdGe}_3\text{O}_2\text{S}_8$  respectively. Notably, the measured  $\Delta n$  values for  $\text{Ba}_3\text{MnGe}_3\text{O}_2\text{S}_8$  and  $\text{Ba}_3\text{CdGe}_3\text{O}_2\text{S}_8$  were found to be 0.11 and 0.14, respectively, using the formula  $\Delta n = R/T$  (Fig. 3).<sup>41</sup> These values are larger than those of commercial materials like  $\text{MgF}_2$  (0.012 @ 632 nm)<sup>42</sup> and  $\text{LiNbO}_3$  (0.08 @ 632 nm),<sup>43</sup> as well as many recently reported chalcogenides, such as  $[\text{Ba}_4(\text{S}_2)][\text{ZnGa}_4\text{S}_{10}]$  (0.053 @ 1064 nm),<sup>44</sup>  $\text{LiBaSbS}_3$  (0.045 at 532 nm),<sup>45</sup> and  $\text{K}_2\text{Na}_2\text{Sn}_3\text{S}_8$  (0.070 at 546 nm).<sup>46</sup> This indicates that the target compounds have potential as birefringent materials. Moreover, it is noteworthy that compared to the 3D  $\text{AE}_3\text{M}^{\text{II}}\text{M}_2^{\text{IV}}\text{Q}_8$  with a  $\Delta n$  value of 0, the 1D  $\text{Ba}_3\text{M}^{\text{II}}\text{Ge}_3\text{O}_2\text{S}_8$  ( $\text{M}^{\text{II}} = \text{Mn, Cd}$ ) oxychalcogenides displayed appropriate  $\Delta n$  values. These findings indicate that the hetero-anion-introduction strategy is effective in increasing optical anisotropy and boosting  $\Delta n$  in the oxychalcogenide family.

For a more comprehensive understanding of the electronic structures and optical performances of  $\text{Ba}_3\text{M}^{\text{II}}\text{Ge}_3\text{O}_2\text{S}_8$  ( $\text{M}^{\text{II}} = \text{Mn, Cd}$ ), detailed theoretical calculations were conducted using the DFT method. As depicted in Fig. S8† and Fig. 4a,  $\text{Ba}_3\text{MnGe}_3\text{O}_2\text{S}_8$  and  $\text{Ba}_3\text{CdGe}_3\text{O}_2\text{S}_8$  exhibited direct band gaps, with calculated  $E_g$  values of 1.53 and 2.47 eV, respectively. These values were notably different from the tested values obtained from the UV-vis-NIR spectra (3.39 and 3.82 eV). This

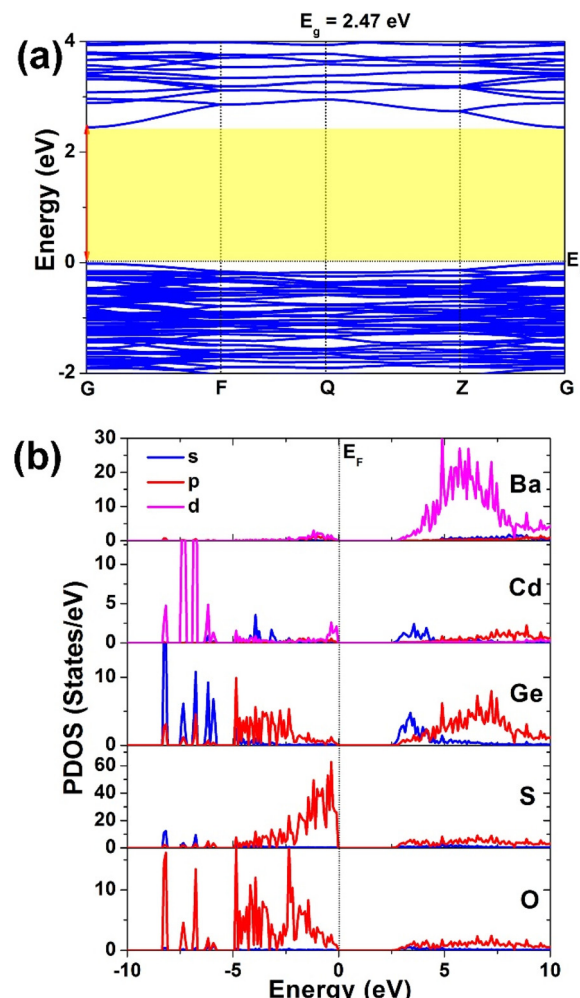


Fig. 4 Theoretical calculated results of  $\text{Ba}_3\text{CdGe}_3\text{O}_2\text{S}_8$ : (a) electronic band structure; (b) PDOS curve.

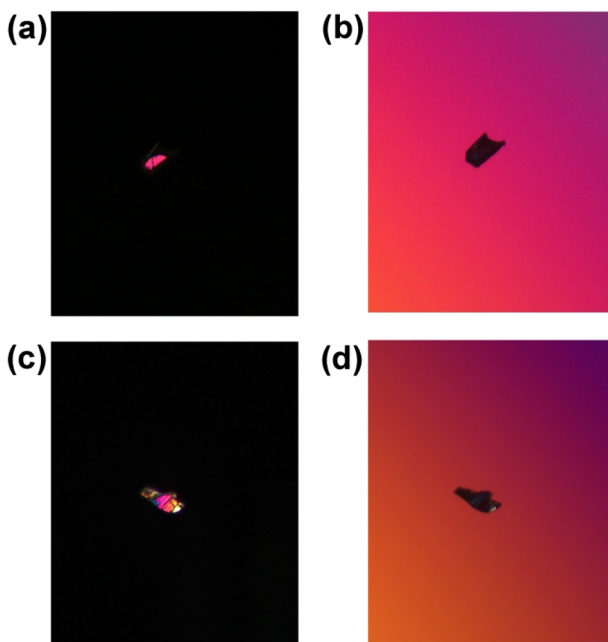
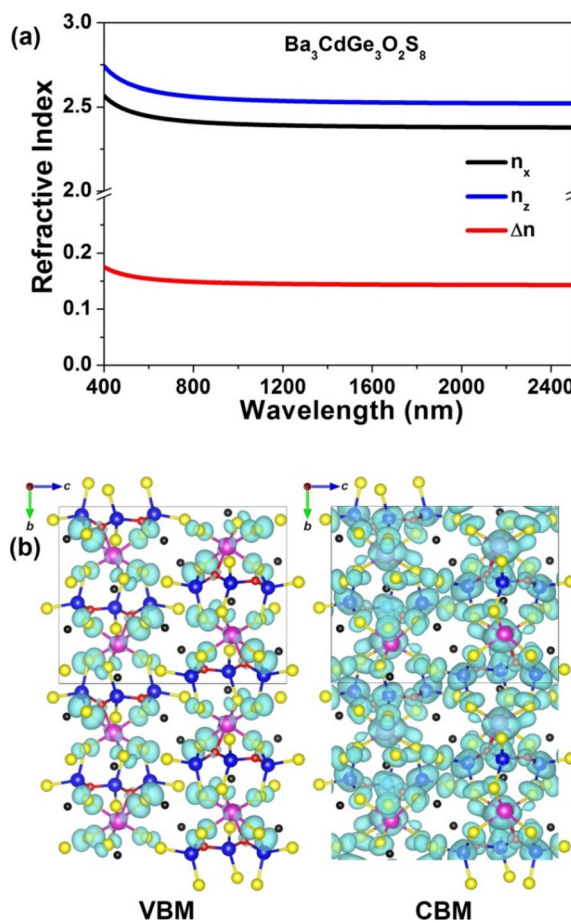


Fig. 3 (a and b)  $\text{Ba}_3\text{MnGe}_3\text{O}_2\text{S}_8$  and (c and d)  $\text{Ba}_3\text{CdGe}_3\text{O}_2\text{S}_8$  crystals for birefringence determination and the interference colors observed before and after complete extinction.

discrepancy may be attributed to the limited accuracy of the conventional DFT functional in describing band gaps.<sup>47</sup> A detailed Brillouin zone plot with high symmetry points is provided in Fig. S9.† Since the  $\text{Ba}_3\text{MnGe}_3\text{O}_2\text{S}_8$  and  $\text{Ba}_3\text{CdGe}_3\text{O}_2\text{S}_8$  compounds demonstrated similarities in the partial density of states (PDOS) curves (Fig. 4b and S8†),  $\text{Ba}_3\text{CdGe}_3\text{O}_2\text{S}_8$  was chosen as the representative compound for further elucidation. In the PDOS graphs, the valence band maximum (VBM) was defined by the S-3p and O-2p nonbonding states, while the conduction band minimum (CBM) was dominated by the unoccupied Cd-4s, Ge-3s, and Ba-4p orbitals. Thus, the  $E_g$  of  $\text{Ba}_3\text{CdGe}_3\text{O}_2\text{S}_8$  was primarily determined by the heteroanionic  $[\text{GeOS}_3]$ ,  $[\text{GeOS}_3]$  and  $[\text{CdOS}_3]$  FBUs, namely, 1D  $[\text{CdGe}_3\text{O}_2\text{S}_8]^{6-}$  chains.

Besides, based on DFT calculations, the  $\Delta n$  of  $\text{Ba}_3\text{M}^{\text{II}}\text{Ge}_3\text{O}_2\text{S}_8$  ( $\text{M}^{\text{II}} = \text{Mn, Cd}$ ) was also calculated (Fig. 5a and S10†). The results reveal that the calculated  $\Delta n$  of  $\text{Ba}_3\text{CdGe}_3\text{O}_2\text{S}_8$  was 0.15 @ 2050 nm. Additionally, when combined with the analysis by the partial charge density graphs in the VBM and CBM ranges (Fig. 5b), it was evident that the het-



**Fig. 5** (a) Calculated refractive index dispersion curves and birefringence of  $\text{Ba}_3\text{CdGe}_3\text{O}_2\text{S}_8$ ; (b) distribution of the partial charge density maps in the VBM and CBM parts. Black atoms: Ba; pink atoms: Cd; blue atoms: Ge; yellow atoms: S; red atoms: O.

heteroanionic FBUs play a significant role in achieving a large  $\Delta n$ . This implies that the introduction of heteroanions into the structure is favorable to the structural anisotropy.

### 3. Conclusions

With the aim of obtaining new IR birefringent materials in the AE-TM-M<sup>IV</sup>-O-Q system, two novel oxychalcogenides  $\text{Ba}_3\text{M}^{\text{II}}\text{Ge}_3\text{O}_2\text{S}_8$  ( $\text{M}^{\text{II}} = \text{Mn}$  or  $\text{Cd}$ ) were successfully synthesized by employing a heteroanion-introduction strategy of replacing part of the Q atoms from the parent  $\text{AE}_3\text{M}^{\text{II}}\text{M}_2^{\text{IV}}\text{Q}_8$ . This is the first case that contains multiple heteroanionic ligands in oxychalcogenides, and the 1D anionic  $[\text{M}^{\text{II}}\text{Ge}_3\text{O}_2\text{S}_8]^{6-}$  chain is exclusively constructed by three heteroanionic units, that is, octahedral  $[\text{M}^{\text{II}}\text{OS}_5]$ , and tetrahedral  $[\text{GeOS}_3]$  and  $[\text{GeO}_2\text{S}_2]$ . Both compounds exhibited a large  $E_g$  (3.39 and 3.82 eV), a broad IR transparency region (2.5–13.3  $\mu\text{m}$ ), and good thermal stability (approximately 1100 K). Specifically,  $\text{Ba}_3\text{M}^{\text{II}}\text{Ge}_3\text{O}_2\text{S}_8$  ( $\text{M}^{\text{II}} = \text{Mn}$  or  $\text{Cd}$ ) demonstrated a large  $\Delta n$  (0.11 and 0.14 @ 549 nm), implying its potential application as an IR birefrin-

gent candidate. Analysis of their structure–property relationships displayed that the 1D chains in a reversed arrangement is favorable for generating a large  $\Delta n$ . Overall, this study represents significant progress in the field of IR birefringent materials and presents a new paradigm for developing crystal structures with enhanced  $\Delta n$  that are suitable for optoelectronic applications.

### Author contributions

Sheng-Hua Zhou: investigation, methodology, validation, writing – original draft. Mao-Yin Ran: investigation, formal analysis, writing – original draft. Wen-Bo Wei: formal analysis, validation. A-Yang Wang: formal analysis, validation. Xin-Tao Wu: conceptualization, writing – review & editing. Hua Lin: supervision, conceptualization, writing – review & editing. Qi-Long Zhu: supervision, writing – review & editing.

### Conflicts of interest

There are no conflicts to declare.

### Acknowledgements

This research was supported by the National Natural Science Foundation of China (21771179), Fujian Science & Technology Innovation Laboratory for Optoelectronic Information of China (2021ZR118), and the Natural Science Foundation of Fujian Province (2022L3092 and 2023H0041).

### References

- 1 (a) Z. Xie, L. Sun, G. Han and Z. Gu, Optical Switching of a Birefringent Photonic Crystal, *Adv. Mater.*, 2008, **20**, 3601–3604; (b) N. Berti, S. Coen, M. Erkintalo and J. Fatome, Extreme waveform compression with a nonlinear temporal focusing mirror, *Nat. Photonics*, 2022, **16**, 822–827; (c) Y. Zhou, X. Zhang, M. Hong, J. Luo and S. Zhao, Achieving effective balance between bandgap and birefringence by confining  $\pi$ -conjugation in an optically anisotropic crystal, *Sci. Bull.*, 2022, **67**, 2276–2279; (d) M. Mutailipu, J. Han, Z. Li, F. M. Li, J. J. Li, F. F. Zhang, X. F. Long, Z. H. Yang and S. L. Pan, Achieving the full-wavelength phase-matching for efficient nonlinear optical frequency conversion in  $\text{C}(\text{NH}_2)_3\text{BF}_4$ , *Nat. Photonics*, 2023, **17**, 694–701; (e) F. Zhang, X. Chen, M. Zhang, W. Jin, S. Han, Z. Yang and S. Pan, An excellent deep-ultraviolet birefringent material based on  $[\text{BO}_2]_\infty$  infinite chains, *Light: Sci. Appl.*, 2022, **11**, 252; (f) X. Dong, L. Huang, H. Zeng, Z. Lin, K. M. Ok and G. Zou, High-Performance Sulfate Optical Materials Exhibiting Giant Second Harmonic Generation and Large Birefringence, *Angew. Chem., Int. Ed.*, 2022, **61**, e202116790; (g) P.-F. Li, C.-L. Hu,

F. Kong and J.-G. Mao, The First UV Nonlinear Optical Selenite Material: Fluorination Control in  $\text{CaYF}(\text{SeO}_3)_2$  and  $\text{Y}_3\text{F}(\text{SeO}_3)_4$ , *Angew. Chem., Int. Ed.*, 2023, **62**, e202301420.

2 H. Luo, T. Tkaczyk, E. Dereniak and K. Oka, High birefringence of the yttrium vanadate crystal in the middle wavelength infrared, *Opt. Lett.*, 2006, **31**, 616–618.

3 G. Ghosh, Dispersion-equation coefficients for the refractive index and birefringence of calcite and quartz crystals, *Opt. Commun.*, 1999, **163**, 95–102.

4 G. Zhou, J. Xu, X. Chen, H. Zhong and F. Gan, Growth and spectrum of a novel birefringent  $\alpha\text{-BaB}_2\text{O}_4$  crystal, *J. Cryst. Growth*, 1998, **191**, 517–519.

5 S. Niu, J. Graham, H. Zhao, Y. Zhou, O. Thomas, H. Huaxun, S. Jad, M. Krishnamurthy, U. Brittany and J. Wu, Giant optical anisotropy in a quasi-one-dimensional crystal, *Nat. Photonics*, 2018, **12**, 392–396.

6 (a) A. Tudi, S. Han, Z. Yang and S. Pan, Potential optical functional crystals with large birefringence: Recent advances and future prospects, *Coord. Chem. Rev.*, 2022, **459**, 214380; (b) Q. Shi, L. Dong and Y. Wang, Evaluating refractive index and birefringence of nonlinear optical crystals: Classical methods and new developments, *Chin. J. Struct. Chem.*, 2023, **42**, 100017; (c) Y. Long, X. Dong, L. Huang, H. Zeng, Z. Lin, L. Zhou and G. Zou,  $\text{BaSb}(\text{H}_2\text{PO}_2)_3\text{Cl}_2$ : An Excellent UV Nonlinear Optical Hypophosphite Exhibiting Strong Second-Harmonic Generation Response, *Mater. Today Phys.*, 2022, **28**, 100876; (d) P.-F. Li, J.-G. Mao and F. Kong, A survey of stereoactive oxysalts for linear and nonlinear optical applications, *Mater. Today Phys.*, 2023, **37**, 101197; (e) P.-F. Li, Y.-P. Gong, C.-L. Hu, B. Zhang, J.-G. Mao and F. Kong, Four UV Transparent Linear and Nonlinear Optical Materials Explored from Pure Selenite Compounds, *Adv. Opt. Mater.*, 2023, **11**, 2301426.

7 (a) X. Y. Zhang, X. G. Du, J. H. Wang, F. Y. Wang, F. Liang, Z. G. Hu, Z. S. Lin and Y. C. Wu,  $\text{K}_3\text{C}_6\text{N}_7\text{O}_3\cdot 2\text{H}_2\text{O}$ : A Multifunctional Nonlinear Optical Cyamelurate Crystal with Colossal  $\pi$ -Conjugated Orbitals, *ACS Appl. Mater. Interfaces*, 2022, **14**, 53074–53080; (b) Y. Li, X. Zhang, J. Zheng, Y. Zhou, W. Huang, Y. Song, H. Wang, X. Song, J. Luo and S. Zhao, A Hydrogen Bonded Supramolecular Framework Birefringent Crystal, *Angew. Chem., Int. Ed.*, 2023, **62**, e202304498.

8 (a) H. Lin, Y. Y. Li, M. Y. Li, Z. J. Ma, L. M. Wu, X. T. Wu and Q. L. Zhu, Centric-to-acentric structure transformation induced by a stereochemically active lone pair: a new insight for design of IR nonlinear optical materials, *J. Mater. Chem. C*, 2019, **7**, 4638–4643; (b) M.-M. Chen, Z. Ma, B.-X. Li, W.-B. Wei, X.-T. Wu, H. Lin and Q.-L. Zhu,  $\text{M}_2\text{As}_2\text{Q}_5$  ( $\text{M} = \text{Ba, Pb}$ ;  $\text{Q} = \text{S, Se}$ ): A source of infrared nonlinear optical materials with excellent overall performance activated by multiple discrete arsenate anions, *J. Mater. Chem. C*, 2021, **9**, 1156–1163; (c) M. M. Chen, S. H. Zhou, W. B. Wei, B. X. Li, M. Y. Ran, X. T. Wu, H. Lin and Q. L. Zhu,  $\text{RbBiP}_2\text{S}_6$ : A Promising IR Nonlinear Optical Material with a Giant Second-Harmonic Generation Response Designed by Aliovalent Substitution, *ACS Mater. Lett.*, 2022, **4**, 1264–1269; (d) S. Han, A. Tudi, W. Zhang, X. Hou, Z. Yang and S. Pan, Recent Development of Sn(II), Sb(III)-based Birefringent Material: Crystal Chemistry and Investigation of Birefringence, *Angew. Chem., Int. Ed.*, 2023, **62**, e202302025; (e) C. Liu, S.-H. Zhou, C. Zhang, Y.-Y. Shen, X.-Y. Liu, H. Lin and Y. Liu,  $\text{CsCu}_3\text{SbS}_4$ : rational design of a two-dimensional layered material with giant birefringence derived from  $\text{Cu}_3\text{SbS}_4$ , *Inorg. Chem. Front.*, 2022, **9**, 478–484; (f) C. Zhang, M.-Y. Ran, X. Chen, S.-H. Zhou, H. Lin and Y. Liu, Stereochemically active lone-pair-driven giant enhancement of birefringence from three-dimensional  $\text{CsZn}_4\text{Ga}_5\text{Se}_{12}$  to two-dimensional  $\text{CsZnAsSe}_3$ , *Inorg. Chem. Front.*, 2023, **10**, 3367–3374.

9 (a) M. Y. Li, B. X. Li, H. Lin, Z. J. Ma, L. M. Wu, X. T. Wu and Q. L. Zhu,  $\text{Sn}_2\text{Ga}_2\text{S}_5$ : A Polar Semiconductor with Exceptional Infrared Optical Properties Originating from the Combined Effect of Mixed Asymmetric Building Motifs, *Chem. Mater.*, 2019, **31**, 6268–6275; (b) M. Y. Li, Z. J. Ma, B. X. Li, X. T. Wu, H. Lin and Q. L. Zhu,  $\text{HgCuPS}_4$ : An Exceptional Infrared Nonlinear Optical Material with Defect Diamond-like Structure, *Chem. Mater.*, 2020, **32**, 4331–4339; (c) J. Zhou, L. Wang, Y. Chu, H. Wang, S. Pan and J. Li,  $\text{Na}_3\text{SiS}_3\text{F}$ : A Wide Bandgap Fluorothiosilicate with Unique  $\text{SiS}_3\text{F}$  Unit and High Laser-Induced Damage Threshold, *Adv. Opt. Mater.*, 2023, **11**, 2300736.

10 S. Liu, X. Liu, S. Zhao, Y. Liu, L. Li, Q. Ding, Y. Li, Z. Lin, J. Luo and M. Hong, An Exceptional Peroxide Birefringent Material Resulting from  $d\pi$  Interactions, *Angew. Chem., Int. Ed.*, 2020, **59**, 9414–9417.

11 J. Guo, A. Tudi, S. Han, Z. Yang and S. Pan,  $\text{Sn}_2\text{PO}_4\text{I}$ : an excellent birefringent material with giant optical anisotropy in non  $\pi$ -conjugated phosphate, *Angew. Chem., Int. Ed.*, 2021, **60**, 24901–24904.

12 Y. Hu, C. Wu, X. Jiang, Z. Wang, Z. Huang, Z. Lin, X. Long, M. G. Humphrey and C. Zhang, Giant Second-Harmonic Generation Response and Large Band Gap in the Partially Fluorinated Mid-Infrared Oxide  $\text{RbTeMo}_2\text{O}_8\text{F}$ , *J. Am. Chem. Soc.*, 2021, **143**, 12455–12459.

13 Y. Deng, L. Huang, X. Dong, L. Wang, K. M. Ok, H. Zeng, Z. Lin and G. Zou,  $\text{K}_2\text{Sb}(\text{P}_2\text{O}_7)\text{F}$ : Cairo pentagonal layer with bifunctional genes reveal optical performance, *Angew. Chem., Int. Ed.*, 2020, **59**, 21151–21156.

14 (a) H. Lin, W. B. Wei, H. Chen, X. T. Wu and Q. L. Zhu, Rational design of infrared nonlinear optical chalcogenides by chemical substitution, *Coord. Chem. Rev.*, 2020, **406**, 213150; (b) Y. F. Shi, W. Wei, X. T. Wu, H. Lin and Q. L. Zhu, Recent progress in oxychalcogenides as IR nonlinear optical materials, *Dalton Trans.*, 2021, **50**, 4112–4118; (c) M. Y. Ran, A. Y. Wang, W. B. Wei, X. T. Wu, H. Lin and Q. L. Zhu, Recent progress in the design of IR nonlinear optical materials by partial chemical substitution: structural evolution and performance optimization, *Coord. Chem. Rev.*, 2023, **481**, 215059; (d) H. D. Yang, M. Y. Ran, W. B. Wei, X. T. Wu, H. Lin and Q. L. Zhu, Recent advances

in IR nonlinear optical chalcogenides with well-balanced comprehensive performance, *Mater. Today Phys.*, 2023, **35**, 101127.

15 M. Sun, X. Zhang, C. Li, W. Liu, Z. Lin and J. Yao, Highly polarized  $[\text{GeOTe}_3]$  motif-driven structural order promotion and an enhanced second harmonic generation response in the new nonlinear optical oxytelluride  $\text{Ba}_3\text{Ge}_2\text{O}_4\text{Te}_3$ , *J. Mater. Chem. C*, 2022, **10**, 150–159.

16 M. Y. Ran, Z. J. Ma, H. Chen, B. X. Li, X. T. Wu, H. Lin and Q. L. Zhu, Partial Isovalent Anion Substitution to Access Remarkable Second-Harmonic Generation Response: A Generic and Effective Strategy for Design of Infrared Nonlinear Optical Materials, *Chem. Mater.*, 2020, **32**, 5890–5896.

17 (a) M. Y. Ran, S. H. Zhou, B. Li, W. Wei, X. T. Wu, H. Lin and Q. L. Zhu, Enhanced Second-Harmonic-Generation Efficiency and Birefringence in Melilite Oxychalcogenides  $\text{Sr}_2\text{MGe}_2\text{OS}_6$  ( $\text{M} = \text{Mn, Zn, and Cd}$ ), *Chem. Mater.*, 2022, **34**, 3853–3861; (b) R. Wang, F. Liang, X. Liu, Y. Xiao, Q. Liu, X. Zhang, L. M. Wu, L. Chen and F. Huang, Heteroanionic Melilite Oxsulfide: A Promising Infrared Nonlinear Optical Candidate with a Strong Second-Harmonic Generation Response, Sufficient Birefringence, and Wide Bandgap, *ACS Appl. Mater. Interfaces*, 2022, **14**, 23645–23652.

18 M. Y. Ran, S. H. Zhou, W. Wei, B. Li, X. T. Wu, H. Lin and Q. L. Zhu, Rational Design of a Rare-Earth Oxychalcogenide  $\text{Nd}_3[\text{Ga}_3\text{O}_3\text{S}_3][\text{Ge}_2\text{O}_7]$  with Superior Infrared Nonlinear Optical Performance, *Small*, 2023, **19**, 2300248.

19 Y. Cheng, H. Wu, H. Yu, Z. Hu, J. Wang and Y. Wu, Rational Design of a Promising Oxychalcogenide Infrared Nonlinear Optical Crystal, *Chem. Sci.*, 2022, **13**, 5305–5310.

20 (a) N. Zhen, K. Wu, Y. Wang, Q. Li, W. H. Gao, D. W. Hou, Z. H. Yang, H. D. Jiang, Y. J. Dong and S. L. Pan,  $\text{BaCdSn}_4$  and  $\text{Ba}_3\text{CdSn}_2\text{S}_8$ : syntheses, structures, and non-linear optical and photoluminescence properties, *Dalton Trans.*, 2016, **45**, 10681; (b) R. H. Duan, P. F. Liu, H. Lin, Y. J. Zheng, J. S. Yu, X. T. Wu, S. X. Huang-Fu and L. Chen,  $\text{Ba}_6\text{Li}_2\text{CdSn}_4\text{S}_{16}$ : lithium substitution simultaneously enhances band gap and SHG intensity, *J. Mater. Chem. C*, 2017, **5**, 7067; (c) R.-H. Duan, R.-A. Li, P.-F. Liu, H. Lin, Y. Wang and L.-M. Wu, Modifying Disordered Sites with Rational Cations to Regulate Band-Gaps and Second Harmonic Generation Responses Markedly:  $\text{Ba}_6\text{Li}_2\text{ZnSn}_4\text{S}_{16}$  vs  $\text{Ba}_6\text{Ag}_2\text{ZnSn}_4\text{S}_{16}$  vs  $\text{Ba}_6\text{Li}_{2.67}\text{Sn}_{4.33}\text{S}_{16}$ , *Cryst. Growth Des.*, 2018, **18**, 5609; (d) Y. Yang, M. Song, J. Zhang, L. Gao, X. Wu and K. Wu, Coordinated regulation on critical physicochemical performances activated from mixed tetrahedral anionic ligands in new series of  $\text{Sr}_6\text{A}_4\text{M}_4\text{S}_{16}$  ( $\text{A} = \text{Ag, Cu; M} = \text{Ge, Sn}$ ) nonlinear optical materials, *Dalton Trans.*, 2020, **49**, 3388; (e) Y. K. Lian, R. A. Li, X. Liu, L. M. Wu and L. Chen,  $\text{Sr}_6(\text{Li}_2\text{Cd})\text{A}_4\text{S}_{16}$  ( $\text{A} = \text{Ge, Sn}$ ): How to Go beyond the Band Gap Limitation via Site-Specific Modification, *Cryst. Growth Des.*, 2020, **20**, 8084; (f) G. Cicirello, K. Wu and J. Wang, Synthesis, crystal structure, linear and non-linear optical properties of quaternary sulfides  $\text{Ba}_6(\text{Cu}_2\text{X})\text{Ge}_4\text{S}_{16}$  ( $\text{X} = \text{Mg, Mn, Cd}$ ), *J. Solid State Chem.*, 2021, **300**, 122226; (g) H. Chen, M. Y. Ran, W. B. Wei, X. T. Wu, H. Lin and Q. L. Zhu, A comprehensive review on metal chalcogenides with three-dimensional frameworks for infrared nonlinear optical applications, *Coord. Chem. Rev.*, 2022, **470**, 214706.

21 (a) M. Zhou, C. Li, X. Li, J. Yao and Y. Wu,  $\text{K}_2\text{Sn}_2\text{ZnSe}_6$ ,  $\text{Na}_2\text{Ge}_2\text{ZnSe}_6$ , and  $\text{Na}_2\text{In}_2\text{GeSe}_6$ : A New Series of Quaternary Selenides with Intriguing Structural Diversity and Nonlinear Optical Properties, *Dalton Trans.*, 2016, **45**, 7627–7633; (b) M. Y. Li, Y. X. Zhang, H. Lin, Z. J. Ma, X. T. Wu and Q. L. Zhu, Combined experimental and theoretical investigations of  $\text{Ba}_3\text{GaS}_4\text{I}$ : interesting structure transformation originated from the halogen substitution, *Dalton Trans.*, 2019, **48**, 17588–17593; (c) M. Y. Ran, Z. Ma, X. T. Wu, H. Lin and Q. L. Zhu,  $\text{Ba}_2\text{Ge}_2\text{Te}_5$ : a ternary NLO-active telluride with unusual one-dimensional helical chains and giant second-harmonic-generation tensors, *Inorg. Chem. Front.*, 2021, **8**, 4838–4845; (d) Q. Wu, C. Yang, X. Liu, J. Ma, F. Liang and Y. Du, Dimensionality reduction made high-performance mid-infrared nonlinear halide crystal, *Mater. Today Phys.*, 2021, **21**, 100569; (e) C. Zhang, S. H. Zhou, Y. Xiao, H. Lin and Y. Liu, Interesting dimensional transition through changing cations as the trigger in multinary thioarsenates displaying variable photocurrent response and optical anisotropy, *Inorg. Chem. Front.*, 2022, **9**, 5820–5827.

22 (a) H. Lin, L. J. Zhou and L. Chen, Sulfides with Strong Nonlinear Optical Activity and Thermochromism:  $\text{ACd}_4\text{Ga}_5\text{S}_{12}$  ( $\text{A} = \text{K, Rb, Cs}$ ), *Chem. Mater.*, 2012, **24**, 3406–3414; (b) H. Lin, L. Chen, L. J. Zhou and L. M. Wu, Functionalization Based on the Substitutional Flexibility: Strong Middle IR Nonlinear Optical Selenides  $\text{AX}_4^{\text{II}}\text{X}_5^{\text{III}}\text{Se}_{12}$ , *J. Am. Chem. Soc.*, 2013, **135**, 12914–12921; (c) Y. J. Zheng, Y. F. Shi, C. B. Tian, H. Lin, L. M. Wu, X. T. Wu and Q. L. Zhu, An Unprecedented Pentanary Chalcohalide with the Mn Atoms in Two Chemical Environments: Unique Bonding Characteristics and Magnetic Properties, *Chem. Commun.*, 2019, **55**, 79–82.

23 M. Sun, W. Xing, M. Lee and J. Yao, Bridging oxygen atoms in trigonal prism units driven strong second-harmonic-generation efficiency in  $\text{Sr}_3\text{Ge}_2\text{O}_4\text{Te}_3$ , *Chem. Commun.*, 2022, **58**, 11167–11170.

24 B. Liu, X. Jiang, G. Wang, H. Zeng, M. Zhang, S. Li, W. Guo and G. Guo, Oxychalcogenide  $\text{BaGeOSe}_2$ : Highly Distorted Mixed-Anion Building Units Leading to a Large Second-Harmonic Generation Response, *Chem. Mater.*, 2015, **27**, 8189–8192.

25 (a) X. Zhang, Y. Xiao, R. Wang, P. Fu, C. Zheng and F. Huang, Synthesis, crystal structures and optical properties of noncentrosymmetric oxsulfides  $\text{AeGeS}_2\text{O}$  ( $\text{Ae} = \text{Sr, Ba}$ ), *Dalton Trans.*, 2019, **48**, 14662–14668; (b) H. D. Yang, S. H. Zhou, M. Y. Ran, X. T. Wu, H. Lin and Q. L. Zhu, Oxychalcogenides as Promising Ultraviolet Nonlinear Optical Candidates: Experimental and Theoretical Studies of  $\text{AeGeOS}_2$  ( $\text{AE} = \text{Sr and Ba}$ ), *Inorg. Chem.*, 2022, **61**, 15711–15720.

26 (a) N. Zhang, Q. Xu, Z. Shi, M. Yang and S. Guo, Characterizations and Nonlinear-Optical Properties of Pentanary Transition-Metal Oxysulfide  $\text{Sr}_2\text{CoGe}_2\text{OS}_6$ , *Inorg. Chem.*, 2022, **61**, 17002–17006; (b) H. D. Yang, S. H. Zhou, M. Y. Ran, X. T. Wu, H. Lin and Q. L. Zhu, Melilite oxychalcogenide  $\text{Sr}_2\text{FeGe}_2\text{OS}_6$ : a phase-matching IR nonlinear optical material realized by isomorphous substitution, *Inorg. Chem. Front.*, 2023, **10**, 2030.

27 W. Xing, P. Fang, N. Wang, Z. Li, Z. Lin, J. Yao, W. Yin and B. Kang, Two Mixed-Anion Units of  $[\text{GeOSe}_3]$  and  $[\text{GeO}_3\text{S}]$  Originating from Partial Isovalent Anion Substitution and Inducing Moderate Second Harmonic Generation Response and Large Birefringence, *Inorg. Chem.*, 2020, **59**, 16716–16724.

28 S. Cui, H. Wu, Z. Hu, J. Wang, Y. Wu and H. Yu, The Antiperovskite-Type Oxychalcogenides  $\text{Ae}_3\text{Q}[\text{GeOQ}_3]$  ( $\text{Ae} = \text{Ba, Sr; Q = S, Se}$ ) with Large Second Harmonic Generation Responses and Wide Band Gaps, *Adv. Sci.*, 2022, **10**, 2204755.

29 (a) Y. Y. Li, W. J. Wang, H. Wang, H. Lin and L. M. Wu, Mixed-Anion Inorganic Compounds: A Favorable Candidate for Infrared Nonlinear Optical Materials, *Cryst. Growth Des.*, 2019, **19**, 4172–4192; (b) H. Chen, W. B. Wei, H. Lin and X. T. Wu, Transition-metal-based chalcogenides: A rich source of infrared nonlinear optical materials, *Coord. Chem. Rev.*, 2021, **448**, 214154; (c) J. J. Xu and K. Wu, Comprehensive review on multiple mixed-anion ligands, physicochemical performances and application prospects in metal oxysulfides, *Coord. Chem. Rev.*, 2023, **486**, 215139.

30 T. Sambrook, C. F. Smura, S. J. Clarke, K. M. Ok and P. S. Halasyaman, Vertex-Linked  $\text{ZnO}_2\text{S}_2$  Tetrahedra in the Oxysulfide  $\text{BaZnOS}$ : a New Coordination Environment for Zinc in a Condensed Solid, *Inorg. Chem.*, 2007, **46**, 2571–2574.

31 Y. Tsujimoto, C. A. Juillerat, W. G. Hang, K. Fujii, M. Yashima, S. Halasyamani and H. Z. Loya, Function of Tetrahedral  $\text{ZnS}_3\text{O}$  Building Blocks in the Formation of  $\text{SrZn}_2\text{S}_2\text{O}$ : A Phase Matchable Polar Oxysulfide with a Large Second Harmonic Generation Response, *Chem. Mater.*, 2018, **30**, 6486–6493.

32 M. Valldor, U. Rößler, Y. Prots, C. Kuo, J. Chiang, Z. Hu, T. Pi, R. Kniep and L. Tjeng, Synthesis and characterization of  $\text{Ba}[\text{CoSO}]$ : magnetic complexity in the presence of chalcogen ordering, *Chem. – Eur. J.*, 2015, **21**, 10821–10828.

33 A. Reshak, Spin-polarized second harmonic generation from the antiferromagnetic  $\text{CaCoSO}$  single crystal, *Sci. Rep.*, 2017, **7**, 46415.

34 J. B. Litteer, J. C. Fettinger and B. W. Eichhorn,  $\text{Ba}_6\text{V}_4\text{O}_5\text{S}_{11}$ , *Acta Crystallogr., Sect. C: Cryst. Struct. Commun.*, 1997, **53**, 163–165.

35 Y. F. Shi, X. F. Li, Y. X. Zhang, H. Lin, Z. Ma, L. M. Wu, X. T. Wu and Q. L. Zhu,  $[(\text{Ba}_{19}\text{Cl}_4)(\text{Ga}_6\text{Si}_{12}\text{O}_{42}\text{S}_8)]$ : a Two-Dimensional Wide-Band-Gap Layered Oxysulfide with Mixed-Anion Chemical Bonding and Photocurrent Response, *Inorg. Chem.*, 2019, **58**, 6588–6592.

36 (a) P. Kubelka, Ein Beitrag zur Optik der farbanstriche, *J. Tech. Phys.*, 1931, **12**, 593; (b) M. A. Butler, Photoelectrolysis and physical properties of the semiconducting electrode  $\text{WO}_2$ , *J. Appl. Phys.*, 1977, **48**, 1914.

37 R. Wang, F. Liang, F. Wang, Y. Guo, X. Zhang, Y. Xiao, K. Bu, Z. Lin, J. Yao, T. Zhai and F. Huang,  $\text{Sr}_6\text{Cd}_2\text{Sb}_6\text{O}_7\text{S}_{10}$ : Strong SHG Response Activated by Highly Polarizable Sb/O/S Groups, *Angew. Chem., Int. Ed.*, 2019, **58**, 8078–8081.

38 X. Lian, Z. T. Lu, W. D. Yao, S. H. Yang, W. Liu, R. L. Tang and S. P. Guo, Structural Transformation and Second-Harmonic-Generation Activity in Rare-Earth and  $d_0$  Transition-Metal Oxysulfides  $\text{RE}_3\text{NbS}_3\text{O}_4$  ( $\text{RE} = \text{Ce, Sm, Gd, Dy}$ ), *Inorg. Chem.*, 2021, **60**, 10885.

39 R. Wang, F. Liang, X. Zhang, Y. Yang and F. Huang, Synthesis, structural evolution and optical properties of a new family of oxychalcogenides  $[\text{Sr}_3\text{VO}_4][\text{MQ}_3]$  ( $\text{M} = \text{Ga, In, Q = S, Se}$ ), *Inorg. Chem. Front.*, 2022, **9**, 4768–4775.

40 (a) Y. Shi, S. Zhou, P. Liu, X. Wu, H. Lin and Q. Zhu, Unique  $[\text{Sb}_6\text{O}_2\text{S}_{13}]^{12-}$  finite chain in oxychalcogenide  $\text{Ba}_6\text{Sb}_6\text{O}_2\text{S}_{13}$  leading to ultra-low thermal conductivity and giant birefringence, *Inorg. Chem. Front.*, 2023, **10**, 4425–4434; (b) H. Liu, Z. Song, H. Wu, Z. Hu, J. Wang, Y. Wu and H. Yu,  $[\text{Ba}_2\text{F}_2][\text{Ge}_2\text{O}_3\text{S}_2]$ : An Unprecedented Heteroanionic Infrared Nonlinear Optical Material Containing Three Typical Anions, *ACS Mater. Lett.*, 2022, **4**, 1593–1598; (c) Y. Shi, Z. Ma, B. Li, X. Wu, H. Lin and Q. Zhu, Phase matching achieved by isomorphous substitution in IR nonlinear optical material  $\text{Ba}_2\text{SnSSi}_2\text{O}_7$  with an undiscovered  $[\text{SnO}_4\text{S}]$  functional motif, *Mater. Chem. Front.*, 2022, **6**, 3054–3061.

41 Y. X. Chen, Z. X. Chen, Y. Zhou, Y. Q. Li, Y. C. Liu, Q. R. Ding, X. Chen, S. G. Zhao and J. H. Luo, An Antimony (III) Fluoride Oxalate With Large Birefringence, *Chem. – Eur. J.*, 2021, **27**, 4557–4560.

42 D. E. Zelmon, D. L. Small and D. Jundt, Infrared corrected Sellmeier coefficients for congruently grown lithium niobate and 5 mol% magnesium oxide-doped lithium niobate, *J. Opt. Soc. Am. B*, 1997, **14**, 3319–3322.

43 M. J. Dodge, Refractive properties of magnesium fluoride, *Appl. Opt.*, 1984, **23**, 1980–1985.

44 K. Ding, H. Wu, Z. Hu, J. Wang, Y. Wu and H. Yu,  $[\text{Ba}_4(\text{S}_2)][\text{ZnGa}_4\text{S}_{10}]$ : Design of an Unprecedented Infrared Nonlinear Salt-Inclusion Chalcogenide with Disulfide-Bonds, *Small*, 2023, **19**, 2302819.

45 A. Abudurusuli, K. Wu, A. Tudi, Z. Yang and S. Pan,  $\text{ABaSbQ}_3$  ( $\text{A} = \text{Li, Na; Q = S, Se}$ ): Diverse Arrangement Modes of Isolated  $\text{SbQ}_3$  Ligands Regulating the Magnitudes of Birefringences, *Chem. Commun.*, 2019, **55**, 5143–5146.

46 X. Ji, H. Wu, B. Zhang, H. Yu, Z. Hu, J. Wang and Y. Wu, Intriguing Dimensional Transition Inducing Variable Birefringence in  $\text{K}_2\text{Na}_2\text{Sn}_3\text{S}_8$  and  $\text{Rb}_3\text{NaSn}_3\text{Se}_8$ , *Inorg. Chem.*, 2021, **60**, 1055–1061.

47 P. E. Blochl, Projector augmented-wave method, *Phys. Rev. B: Condens. Matter*, 1994, **50**, 17953–17979.